INTERNATIONAL JOURNAL OF CLIMATOLOGY
Int. J. Climatol. **34**: 3840–3848 (2014)
Published online 4 March 2014 in Wiley Online Library
(wileyonlinelibrary.com) DOI: 10.1002/joc.3942

RMetS
Royal Meteorological Society

Variation of upper tropospheric clouds and water vapour over the Indian Ocean

Rohini L. Bhawar,[a,b]* Jonathan H. Jiang,[a] Hui Su[a] and Michael J. Schwartz[a]

[a] *Jet Propulsion Laboratory, California Institute of Technology, Pasadena, CA, USA*
[b] *Department of Atmospheric & Space Science, University of Pune, India*

ABSTRACT: The objective of this paper is to understand the response of upper tropospheric (UT) clouds and water vapour (H_2O) to sea surface temperature (SST) changes over the Indian Ocean. UT ice water content (IWC) and H_2O observed by Aura Microwave Limb Sounder (MLS) show dominant dipole mode variability over the Indian Ocean. This is characterized by the oscillating differences between the western and eastern Indian Ocean (WIO and EIO) with greater amplitude in September, October and November (SON) as compared with other seasons. We denote $\delta X = X\_WIO - X\_EIO$, with X being H_2O and IWC at three UT levels (215, 147 and 100 hPa) or SST, following the documented definition for Indian Ocean Dipole (IOD). We find a strong positive correlation between δIWC at the three UT levels and δSST, and a relatively weak positive correlation between δIWC and Niño 3.4 SST, suggesting that the UT clouds over the Indian Ocean are largely controlled by the local thermally driven circulation, while teleconnection to El Niño and Southern Oscillation (ENSO) plays a secondary role. The change per degree of δSST for δIWC in SON is 5.5 mg m^{-3} C^{-1} at 215 hPa, 1.6 mg m^{-3} C^{-1} at 147 hPa and 0.13 mg m^{-3} C^{-1} at 100 hPa (i.e. 96% C^{-1}, 87% C^{-1} and 46% C^{-1} increase at 215, 147 and 100 hPa, respectively). We find 36% C^{-1} increase in δH_2O at 215 hPa with increasing δSST, associated with a sharp contrast in convective strength (indicated by δIWC) over the Indian Ocean region. On the other hand, δH_2O at 100 hPa decreases with increasing δSST because cold temperature is observed above convective clouds and 100 hPa H_2O is largely controlled by temperature. The Niño 3.4 SST has a relatively weak positive (negative) correlation with δH_2O at 215 hPa (100 hPa).

KEY WORDS clouds; variability; Indian Ocean

Received 9 July 2012; Revised 3 January 2014; Accepted 7 January 2014

1. Introduction

The inter-annual variability over the Indian Ocean is influenced by both large-scale dynamics and local Indian Ocean internal dynamics. In recent years, there have been a number of studies on the inter-annual variability in the tropical Indian Ocean (e.g. Perigaud and Delecluse, 1993; Masumoto and Meyers, 1998), with increasing focus on Indian Ocean Dipole (IOD) events (Behera *et al.*, 1999; Saji *et al.*, 1999; Vinayachandran *et al.*, 1999; Webster *et al.*, 1999). The thermal structure of the equatorial Indian Ocean is characterized by warmer (cooler) sea surface temperature (SST) in the east (west) as a consequence of the upwelling along the western boundary and strong eastward equatorial jets that transport warm upper layer water to the east (Vinayachandran *et al.*, 2007). Using observational data over the past 40 years, a pattern of internal variability with anomalously low SST off Sumatra in the eastern Indian Ocean (EIO) and anomalously high SST in the western Indian Ocean (WIO) was identified. This SST anomaly pattern accompanied by coherent wind and precipitation anomalies was reported as the IOD (Saji *et al.*, 1999; Webster *et al.*, 1999). A positive IOD event refers to negative SST anomalies in the EIO and positive SST anomalies in the WIO. This oscillatory mode of coupled ocean–atmosphere variability causes climatic extremes such as droughts in East Asia and Australia and floods in parts of India and East Africa during austral winter and spring (Saji *et al.*, 1999; Meyers *et al.*, 2007).

The issue regarding the relationship between the IOD and the El Niño and Southern Oscillation (ENSO) has been vigorously debated. Cai *et al.* (2012) show that the coherence between the positive IOD and El Niño is much higher than that between negative IOD and La Niña, indicating a potentially greater impact from El Niño compared with La Niña. It is also observed that several significant IOD events have occurred in the absence of ENSO events with the correlation between the dipole mode index (DMI) and the Niño 3 SST index being 0.34 (Saji *et al.*, 1999). The DMI refers to the anomalous SST difference between the WIO and the EIO (Saji *et al.*, 1999). The DMI–Niño 3 correlation increases to 0.56 during the boreal fall. Although this is not a necessary condition for the dependency of two phenomena, a few studies questioned the independence of IOD from ENSO

* Correspondence to: R. L. Bhawar, Department of Atmospheric & Space Science, University of Pune, Pune 411007, India. E-mail: rohinibhawar@gmail.com

(e.g. Baquero-Bernal *et al.*, 2002; Hastenrath, 2002). Cai *et al.* (2012) show that a strong asymmetry does in fact exist in the relationship between the ENSO and the IOD (e.g. during the years 2007 and 2008 positive IOD (pIOD) occurred in conjunction with a La Niña; Cai *et al.*, 2009). The consensus is that while both ENSO and IOD can affect each other, IOD can also occur independently from ENSO (Li *et al.*, 2003; Saji and Yamagata, 2003; Kug and Kang, 2006).

The main aim of this study is to understand the variability of upper tropospheric (UT) ice water content (IWC) and water vapour (H_2O) observed by Aura Microwave Limb Sounder (MLS) in association with SST over the Indian Ocean, with the focus on the variability related to the observed and documented IOD. UT clouds have important radiative effects on the earth-atmosphere system (Liou, 1986). They are closely related to UT humidity, which is the dominant contributor to the greenhouse effect (e.g. Lindzen, 1990; Sun and Lindzen, 1993; Soden and Fu, 1995; Su *et al.*, 2006, 2008, 2009). One of the greatest challenges in climate model simulations and climate change predictions is to accurately represent these UT clouds, their radiative effects and associated climate feedbacks (Cess 1996; Stephens, 2005; Jiang *et al.*, 2012; Su *et al.*, 2013). The UT H_2O and IWC are found closely related to convective strengths (Su *et al.*, 2006; Jiang *et al.*, 2007). Therefore, studying UT H_2O and clouds is useful to infer convective variability which is tied to surface precipitation.

Aura MLS provides unique UT observations of IWC and H_2O at different vertical levels from 215 hPa and above. Thus, in the forthcoming sections we will present the seasonal maps that focus on the observed IOD, the time series of SST and IWC over the two regions over which the dipole pattern oscillates and the correlations of the UT IWC, H_2O and temperature in those regions with local Indian Ocean SST and Niño 3.4 SST. Correlations of these UT observations with SST provide a perspective to understand the dynamical processes involving deep convection and ocean–atmosphere coupling, and local *versus* remote SST influences.

2. Data sets

MLS Level 2, IWC, H_2O and temperature measurements from September 2004 to December 2010 (7 years) and National Center for Environmental Prediction (NCEP) SST and air temperature data for the same period are used for this study. MLS measures ~3500 vertical profiles per day along a sun-synchronous sub-orbital track with equatorial crossings at 1:40PM and 1:40 AM local solar times. The MLS data version 2.2 provides H_2O and IWC above 215 hPa with a vertical resolution of about ~3–4 km (Livesey *et al.*, 2007, Jiang *et al.*, 2010). The MLS H_2O single measurement precision varies from ~25% at 316 hPa to ~10% at 100 hPa, with an expected accuracy of ~10%. For IWC, the precision ranges from ~0.6 to 1.3 mg m^{-3} at 215 hPa, 0.2 mg m^{-3} at 147 hPa and 0.07 mg m^{-3} at 100 hPa (Wu *et al.*, 2008). Estimated measurement accuracy is a factor of two for IWC (Jiang *et al.*, 2010). The MLS temperature at 215 hPa has a cold bias of 1–2 K over the cloudy regions and much smaller biases at higher altitudes (Schwartz *et al.*, 2008). The MLS data have horizontal resolutions of ~200–300 km along-track and ~7 km across-track (Wu *et al.*, 2008).

The SST anomalies were computed relative to the mean over the MLS measurement period from 2004 to 2010. The region considered in the study is the Indian Ocean region 50° to 110°E and 10°S to 10°N. Monthly and seasonal averages have been analysed for UT IWC and H_2O at 215, 147 and 100 hPa pressure levels.

3. Results and discussion

3.1. Seasonal maps

Figure 1(a) and (b) shows the seasonal anomaly maps for June–August (JJA) and September–November (SON) for SST, H_2O and IWC at 215 hPa during the years 2004–2010. The climatological means are constructed for each season from 2004 to 2010. Since MLS observations started in August 2004, JJA maps start from the year 2005. The boxes marked in the SST maps indicate the two regions WIO (50°–70°E and 10°S–10°N) and EIO (90°–110°E and 10°–0°S) between which the dipole pattern oscillates. These boxes are considered from the previous studies (Saji *et al.*, 1999; Webster *et al.*, 1999). In both JJA and SON seasons, positive SST anomalies in the WIO box tend to be associated with positive H_2O and IWC anomalies, accompanied by negative SST, H_2O and IWC anomalies in the EIO box at 215 hPa. During SON in 2006, we observe strong positive H_2O and IWC anomalies in WIO and negative anomalies in EIO, in phase with the SST anomalies, approximately resembling a positive IOD pattern. On the contrary, a strong negative IOD pattern is observed in the year 2010 with positive anomaly for IWC and H_2O in EIO and negative anomaly in WIO. There is no clear periodic oscillation of this dipole pattern during MAM and DJF. The SON months are considered in our analysis as we observe this dipole mode at its peak. During JJA, we observe this dipole mode to be weak and in its starting phase.

3.2. EOF analysis

We performed empirical orthogonal function (EOF) analysis on the monthly MLS IWC anomalies over the Indian Ocean domain and also for the entire tropics for June–November for the period 2004–2010. Using this method, the bulk of the variance of a data set can be described by a few orthogonal modes, so that the dominant/significant modes of variability can be easily identified (Lee *et al.*, 2003). The top panel of Figure 2(a) shows the first three EOF modes over the entire tropics for these 39 monthly samples, while the bottom panel shows the principal components for the leading EOF mode (EOF1) over the entire tropics and over the Indian Ocean along

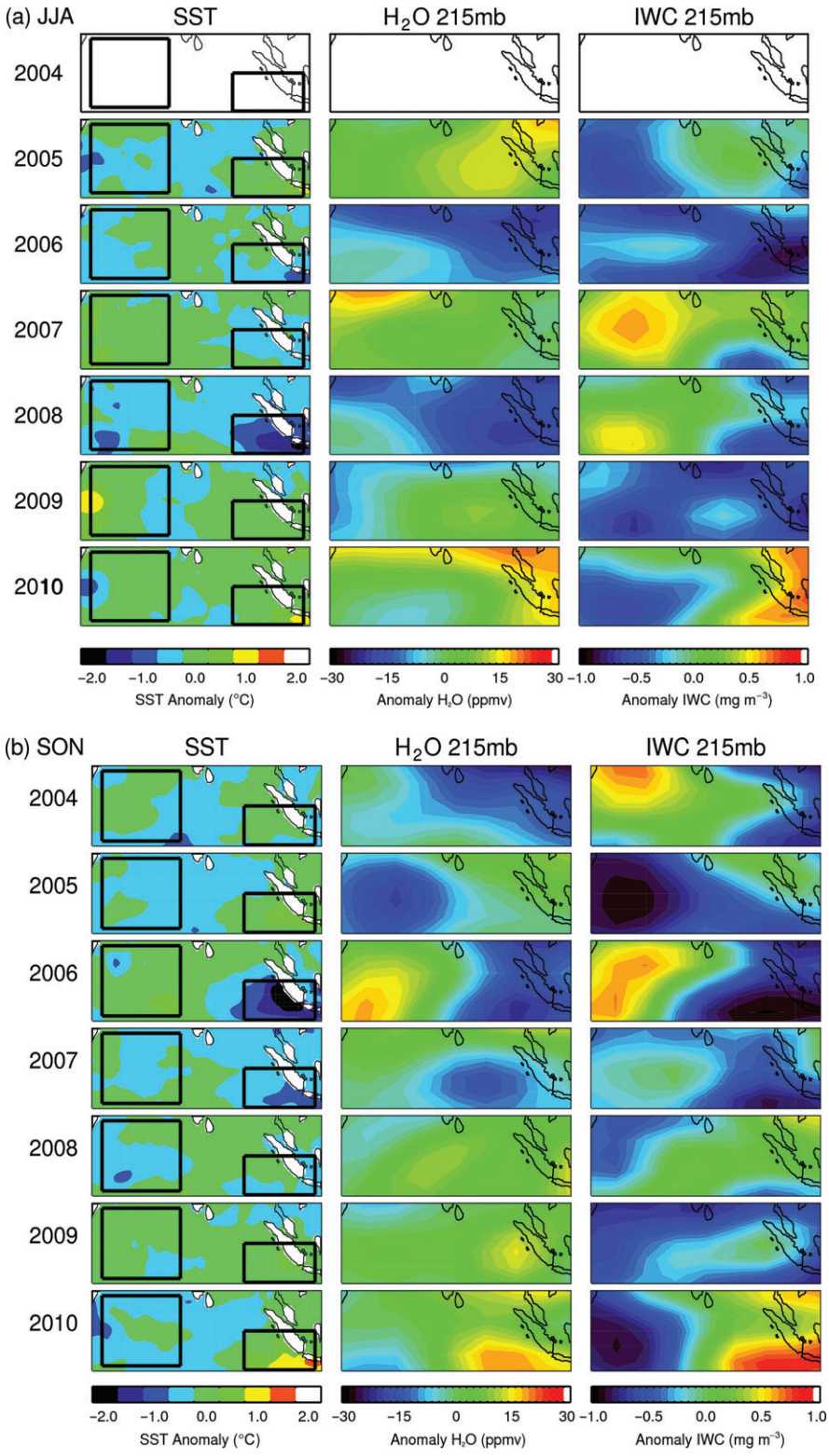

Figure 1. (a) SST, H_2O and IWC anomalies at 215 hPa for June–August (b) SST, H_2O and IWC anomalies for September–November. The boxes indicated in the first column are the WIO (50°–70°E and 10°S–10°N) and EIO (90°–110°E and 10°–0°S) regions.

with the Niño 3.4 SST anomaly time series. The EOF1 explains 12% variance and shows a dipole pattern, while the second and third modes explain 7 and 5% variance, respectively. This confirms that the most significant variability in the Indian Ocean is indeed a dipole pattern. We also carried out the EOF analysis using all the monthly data (76 months) from September 2004 to December 2010 for the Indian Ocean domain (not shown). The dipole mode has 16% variance and the second and third modes explain 11 and 7% variance, respectively. The UT dipole

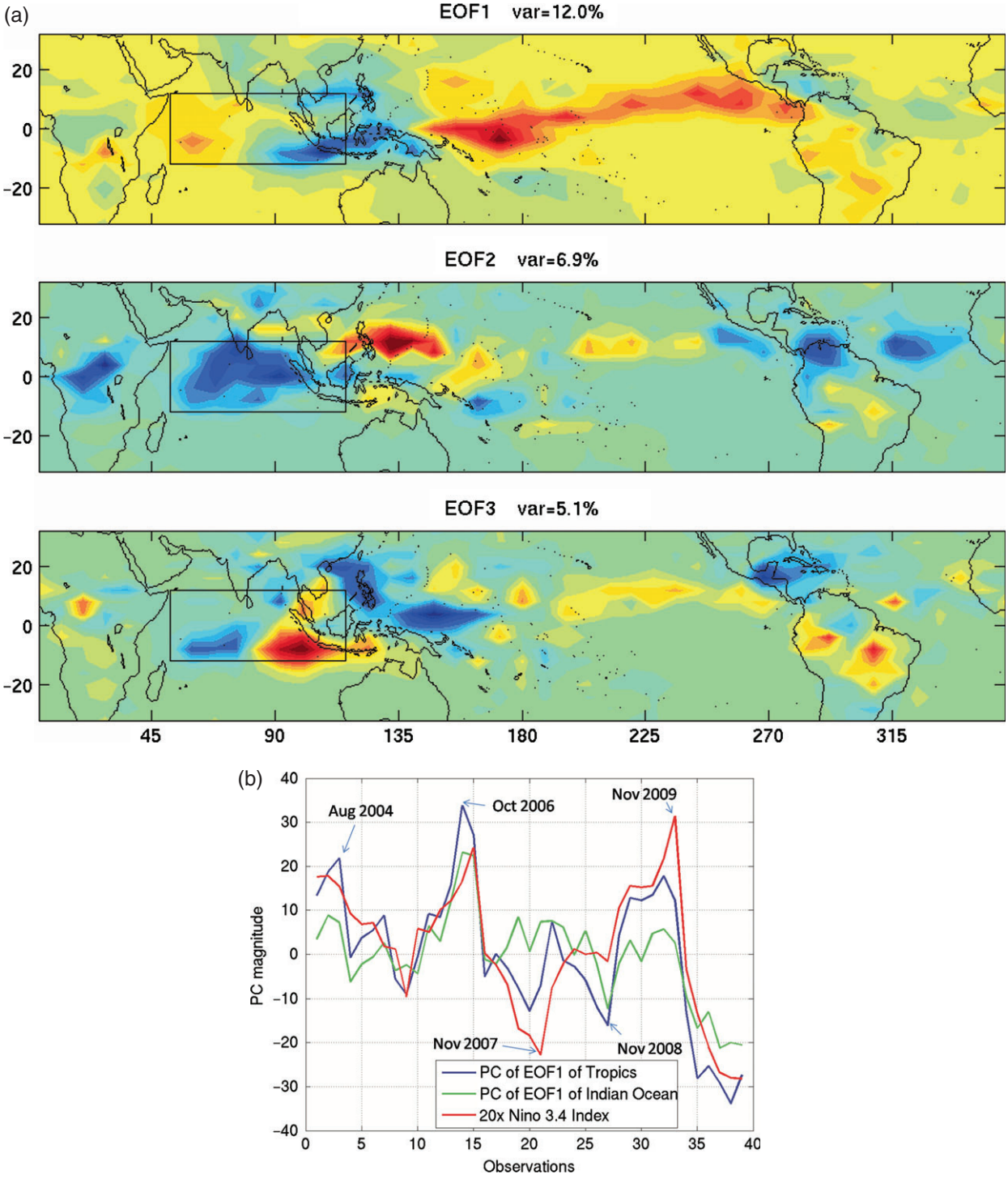

Figure 2. (a) Top panel shows the three EOF modes for entire tropics for IWC at 215 hPa (the boxes marked show the entire IOD region); (b) bottom panel shows the principal components for EOF1 over the entire tropics and over the Indian Ocean along with the Nino 3.4 SST anomaly time series.

mode is found to be an intrinsic mode of the Indian Ocean, though it is correlated with ENSO. We observe that the Niño 3.4 index is very well correlated with the tropical mean SST anomalies, suggesting that the inter-annual anomalies of tropical SST are mostly driven by ENSO (Figure 2(b), lower panel). However, we also observe that there are a few cases when the PCs for EOF1 in the Indian Ocean are not following ENSO.

3.3. Time series of SST and IWC for the dipole mode

The intensity of the IOD is usually represented by the anomalous SST difference between the WIO and the EIO, termed the DMI (Saji *et al.*, 1999). Figure 3(a) shows a time series of DMI calculated over the period of September 2004 to December 2010 with positive DMI corresponding to positive IOD events. The dashed lines at $\pm 0.5\,^{\circ}$C distinguish between the weak (DMI $\leq 0.5\,^{\circ}$C)

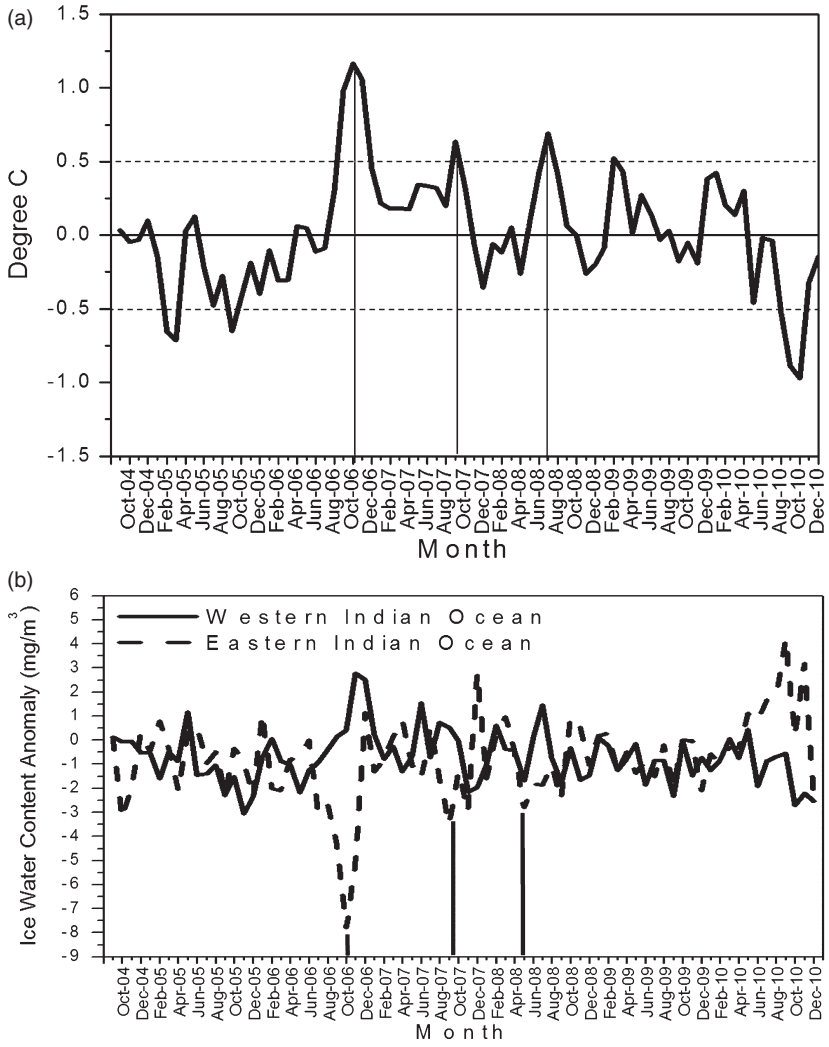

Figure 3. (a) Top panel represents the monthly dipole mode index (DMI) for the period September 2004–December 2010 and (b) bottom panel represents the time series of IWC anomaly at 215 hPa over the western and eastern Indian Ocean boxes.

and strong IOD (DMI $\geq$0.5 °C) events. From September 2004 to December 2010, there are three strong positive IOD events (during 2006, 2007 and 2008) and three strong negative IOD events (two during 2005 and one in 2010). In the year 2006, we see a strong peak of more than 1.0 °C in DMI during October; in 2007, DMI peaked in September and in 2008 it peaked during July and diminished in October. These three consecutive positive IODs are of rare occurrence (Cai *et al.*, 2009). The three strong negative dipole modes peaked in March 2005, September 2005 and October 2010.

Figure 3(b) shows the monthly time series of IWC anomalies at 215 hPa from September 2004 to December 2010 for WIO and EIO separately. An anti-correlation is observed between the WIO and EIO IWCs. The WIO and EIO regions show anti-correlation during the period of SON. The correlation coefficient is found to be −0.41 with 95% statistical significance. The three strong positive IOD events stand out as the troughs over the EIO region and ridges over the WIO region, while the three negative IOD events show approximately opposite responses in the EIO and WIO.

3.4. The relationships of IWC and H_2O with SST

Given that the dipole mode emerges as a significant mode in the inter-annual variability, we define δX as the difference between WIO and EIO, where X is H_2O, IWC or temperature (T) at three UT levels, or SST. The relationships of δIWC, δH_2O and δT with δSST are examined, along with their relationships with Niño3.4 SST anomalies in order to distinguish the local Indian Ocean forcing from the remote Pacific forcing associated with the ENSO.

The top panels of Figure 4 show scatter plots of δIWC, δH_2O and δT at three levels *versus* δSST for SON. The lower panels of Figure 4 show the scatter plots of δIWC, δH_2O and δT *versus* Niño 3.4 SST for SON. Each dot corresponds to a SON average for a certain year (2004–2010). From the scatter plots of δIWC *versus* δSST, we find a strong positive correlation of more than 0.95 (statistical significance level above 99%) for all the three levels at 215, 147 and 100 hPa. This indicates that as δSST increases, the difference in deep convection strength between WIO and EIO increases, leading to a positive δIWC. All the points are clustered

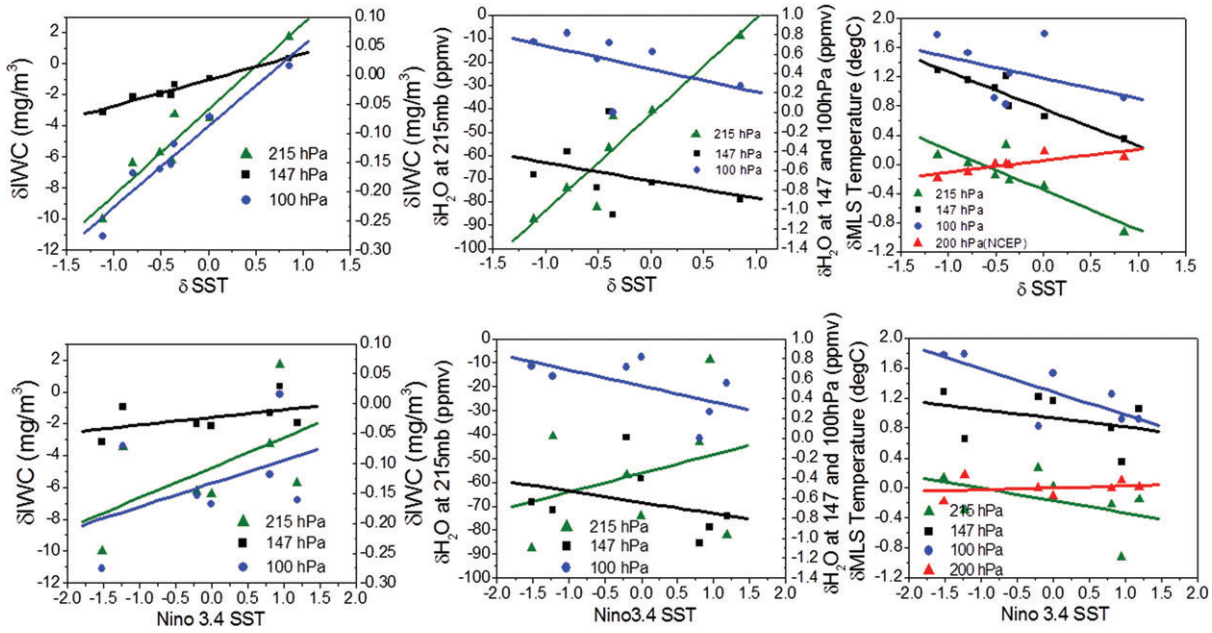

Figure 4. (a) Top panel scatter plots for δIWC, δH_2O and δtemperature *versus* δSST for September–November. (b) Bottom panel scatter plots for δIWC, δH_2O and δtemperature *versus* Nino 3.4 SST for September–November.

Table 1. Slopes and correlation coefficients for IWC and H_2O at three pressure levels 215, 147 and 100 hPa for WIO–EIO box.

September–November values and correlation for West–East Indian Ocean box				
	Ice water content (mg m^{-3} C^{-1})		Water vapour (ppmv C^{-1})	
Levels (hPa)	Values	Correlation	Values	Correlation
		Local SST		
215	5.52	0.96	41.28	0.93
147	1.67	0.97	−0.185	−0.33
100	0.138	0.96	−0.23	−0.51
		Nino 3.4 SST		
215	1.89	0.55	7.81	0.29
147	0.48	0.46	−0.112	−0.34
100	0.03	0.45	−0.161	−0.58

along the linear fit. The rate of increase in δIWC is 5.5 mg m^{-3} C^{-1} at 215 hPa, 1.6 mg m^{-3} C^{-1} at 147 hPa and 0.13 mg m^{-3} C^{-1} at 100 hPa (the 7-year mean δIWC is 4.7, 1.6 and 0.13 mg m^{-3} at 215, 147 and 100 hPa, respectively) as mentioned in Table 1. Su *et al.* (2008) suggest an increase of 15% K^{-1} at 215 hPa, 34% K^{-1} at 147 hPa and 60% K^{-1} at 100 hPa for 15°S–15°N tropical mean IWC during the period from 8 August 2004 to 30 September 2006. We observe 96, 87 and 46% C^{-1} at 215, 147 and 100 hPa, respectively, for the 7-year period 2004–2010. As we are concentrating over a small region, the IOD region, we see strong regional increase at 215 hPa as compared to the percentages reported for the tropical mean (30°N–30°S).

For δH_2O *versus* δSST, we observe a positive correlation of about 0.93 (statistical significance level of 99%) at 215 hPa and a negative correlation of −0.3 (not statistically significant) and −0.5 (above statistical significance of 90%) at 147 and 100 hPa, respectively. The slope of δH_2O *versus* δSST is 41.2 ppmv C^{-1} at 215 hPa, −0.18 ppmv C^{-1} at 147 hPa and −0.23 ppmv C^{-1} at 100 hPa (with 7-year mean δH_2O values of 114.5, 8.7 and 4.08 ppmv at the three levels) as shown in Table 1. We find about 36% C^{-1} change in δH_2O with δSST at 215 hPa. This percentage change in δH_2O with δSST is stronger than those reported in previous studies (30°N–30°S), about 20 and 17% K^{-1}for tropical averages (Su *et al.*, 2006; Luo *et al.*, 2012). This might indicate that the Indian Ocean region has stronger convective activity than the tropics as a whole.

We also plotted the MLS temperature to understand variations in UT water vapour. The strong increase in δH_2O at 215 hPa with δSST is related to the greater convection contrast between WIO and EIO owing to the SST difference. The presence of cold bias in the 215 hPa MLS temperature over the cloudy regions yields a negative δH_2O–δT relation. Hence, we looked at the NCEP air temperature at 200 hPa. The regions with large MLS IWC are generally collocated with regions of low OLR, so that we can use IWC as a good indicator of

deep convection (Su *et al.*, 2006; Jiang *et al.*, 2007). We observe an increase in 215 hPa δH_2O with δSST, in phase with the increase in δIWC and an increase of δT, suggesting that convective transport is predominant in determining the H_2O changes at 215 hPa. Increases in IWC and H_2O and hence in deep convection are associated with an increase in temperature at 215 hPa.

On the other hand, δH_2O at 147 and 100 hPa appears to be negatively correlated with δSST but in phase with δT at the same level. This is consistent with the 'convective cold top' observation and the theory elaborated by Holloway and Neelin (2007). Above the enhanced convection, temperature is usually colder than normal. Hence, positive δSST would cause negative δT in the tropical tropopause layer (TTL). In this layer, especially at 100 hPa, the change in water vapour is primarily governed by change in temperature (Brewer, 1949; Jensen *et al.*, 1996; Liu *et al.*, 2007; Corti *et al.*, 2008; Jiang *et al.*, 2010). We define the level of 147 hPa as a transition level between the convection-dominated 215 hPa to temperature-controlled 100 hPa; thus, δH_2O at this level has a weak correlation with δSST. The change in δH_2O at 100 hPa with δSST is -0.23 and -0.18 ppmv C^{-1} at 147 hPa.

From the correlations of δIWC and δH_2O with δSST, we can clearly see that local Indian Ocean SST strongly governs the UT clouds and water vapour variability via the changes in deep convection. However, previous studies indicate that precipitation (convection) in the Indian Ocean is also impacted by ENSO (e.g. Su *et al.*, 2001, Zhong *et al.*, 2005) through an 'atmospheric bridge' (Alexander, 1992). The bottom panels of Figure 4 show the scatter plots of δIWC, δH_2O and δT at the three UT levels *versus* Nino 3.4 SST anomalies for SON. A positive correlation of about 0.4 (statistically less significant) is found between δIWC and Nino 3.4 SST. The rate of increase in δIWC is 1.9 mg m^{-3} C^{-1} at 215 hPa, 0.48 mg m^{-3} C^{-1} at 147 hPa and 0.03 mg m^{-3} C^{-1} at 100 hPa also indicated in Table 1. For δH_2O, we observe a positive slope of 7.8 ppmv C^{-1} at 215 hPa, and a small negative slope of -0.11 and -0.16 ppmv C^{-1} at 147 and 100 hPa with Nino 3.4 SST, respectively. Thus, there appears to be a positive correlation between the dipole mode and ENSO, though the ENSO influence on the UT water vapour and cloud dipole modes (correlation of 0.4 having very less statistical significance) is significantly weaker than the local SST dipole effect. We also observe a similar relationship during JJA (not shown) to that in SON. We found a negative correlation of δH_2O with Nino 3.4 SST over the EIO region and a positive correlation over the WIO region. We speculate that this negative correlation over EIO is due to the teleconnection from the Pacific over the Indian Ocean. The resultant positive correlation of δH_2O over WIO with Nino 3.4 SST might be due to the coincidental increased convection in the presence of local SST anomalies, as δSST and Nino 3.4 SST have a positive correlation of 0.4.

4. Summary

On the basis of the EOF analysis of 7 years of MLS IWC observations, a dipole mode oscillating between WIO and EIO is found to be the dominant mode in the UT on inter-annual timescales over the Indian Ocean for June–November. The relationships of the UT IWC and H_2O dipoles with the Indian Ocean SST dipole anomaly and with the Nino3.4 SST anomaly over the Pacific Ocean are examined. The teleconnections between ENSO and UT have been mentioned in previous studies (Kent *et al.*, 1995; Wang *et al.*, 1996, Massie *et al.*, 2000). However, the implications of the IOD on the UT have been limited and have been focused over the southern high latitudes and high-frequency atmospheric variability (Liu *et al.*, 2007; Kug *et al.*, 2009). Hence, we put forth our results of the UT IWC and H_2O variability over the IOD domain with SST changes. We found that there are strong positive correlations between the local WIO and EIO SST difference (δSST) and the UT dipole parameters (δIWC, δH_2O and δT). This study estimates an increase in δIWC due to local δSST changes, as well as Niño 3.4 SST anomalies. For δH_2O, we found a strong increase at 215 hPa correlated to local SST dipole anomaly. At 100 hPa, a negative correlation of -0.5 is observed between δH_2O and δSST with a slope of -0.23 ppmv C^{-1}. A similar negative correlation of -0.5 was found between δH_2O and Niño 3.4 SST at 100 hPa with a slope of -0.16 ppmv C^{-1}. The 147 hPa level appears to be a transition between the 215 and 100 hPa levels, with correlations in between the two levels and in phase with those at 100 hPa.

Summarizing the correlations we have examined, Figure 5 schematically illustrates the physical processes that govern the inter-annual variabilities of UT clouds and water vapour observed by MLS. The primary driver for the UT IWC and H_2O dipole modes is the local Indian SST dipole, which induces oppositely phased convective anomalies in the WIO and EIO, causing

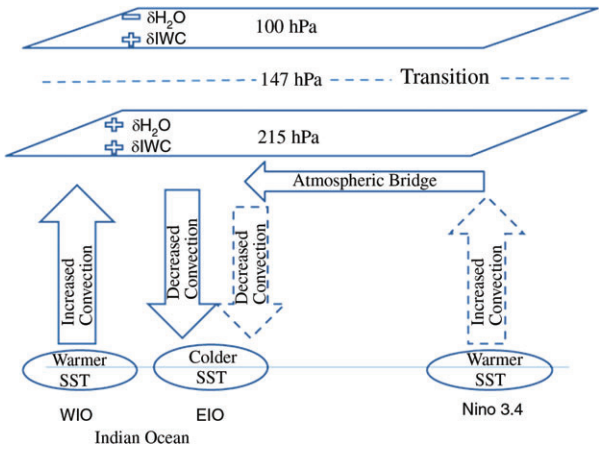

Figure 5. Schematic diagram showing the local and large-scale effects over the Indian Ocean domain (δ refers to WIO – EIO, + means positive correlation with local δSST and – means negative correlation with local δSST).

the dipole patterns in UT IWC and H_2O at 215 hPa. The IWC changes are vertically coherent but H_2O switches sign in the TTL. Above the convection, cold temperature anomalies are produced, leading to negative H_2O anomalies, which is opposite to the positive H_2O anomalies at 215 hPa. The vertical extent of IOD is up to UT, similar to the case of ENSO.

Apart from the local SST influence, the UT over the Indian Ocean is also influenced by the SST anomalies in the eastern/central Pacific Ocean associated with ENSO. During the warm phase of El Niño, anomalously strong convection over the Pacific would cause abnormal subsidence over the Indian Ocean through an 'atmospheric bridge' (dashed arrows). It appears that the forced subsidence over the EIO (in addition to the anomalous subsidence induced by local SST anomalies) strengthens the dipole pattern induced by the local Indian Ocean SST dipole anomalies (solid arrows). However, the influence of this teleconnection on the UT dipole pattern is weaker than the local SST dipole forcing. We suppose there may be an influence on the EIO region through the atmospheric teleconnection from the Pacific. The potential influence of ENSO on the WIO and EIO requires further study.

Acknowledgements

The authors acknowledge the National Centers for Environmental Prediction (NCEP) for the surface parameters. The work was carried out at the Jet Propulsion Laboratory, California Institute of Technology, under contract with NASA. We also thank Dr P. R. C. Rahul and Dr Jennifer Small for helpful comments and reviewing the early versions of this manuscript.

References

Alexander MA. 1992. Midlatitude atmosphere-ocean interaction during El Nino, part I, The North Pacific Ocean. *J. Clim.* **5**: 944–958.

Baquero-Bernal A, Latif M, Legutke S. 2002. On dipole like variability in the tropical Indian Ocean. *J. Clim.* **15**: 1358–1368.

Behera SK, Krishnan R, Yamagata T. 1999. Unusual ocean-atmosphere conditions in the tropical Indian Ocean during 1994. *Geophys. Res. Lett.* **26**: 3001–3004.

Brewer AW. 1949. Evidence for a world circulation provided by the measurements of helium and water vapor distribution in the stratosphere. *Q. J. R. Meteorol. Soc.* **75**: 351–363.

Cai W, Pan A, Roemmich D, Cowan T, Guo X. 2009. Argo profiles a rare occurrence of three consecutive positive Indian Ocean Dipole events, 2006–2008. *Geophys. Res. Lett.* **36**: L08701, DOI: 10.1029/2008GL037038.

Cai W, van Rensch P, Cowan T, Hendon HH. 2012. An asymmetry in the IOD and ENSO teleconnection pathway and its impact on Australian climate. *J. Clim.* **25**: 6318–6329.

Cess RD. 1996. Cloud feedback in atmospheric general circulation models: an update. *J. Geophys. Res.* **101**(D8): 12791–12794.

Corti T, Luo BP, de Reus M, Brunner D, Cairo F, Mahoney MJ, Martucci G, Matthey R, Mitev V, dos Santos FH, Schiller C, Shur G, Sitnikov NM, Spelten N, Vössing HJ, Borrmann S, Peter T. 2008. Unprecedented evidence for deep convection hydrating the tropical stratosphere. *Geophys. Res. Lett.* **35**: L10810, DOI: 10.1029/2008GL033641.

Hastenrath S. 2002. Dipoles, temperature gradient, and tropical climate anomalies. *Bull. Am. Meteorol. Soc.* **83**: 735–738.

Holloway CE, Neelin JD. 2007. The convective cold top and quasi equilibrium. *J. Atmos. Sci.* **64**: 1467–1487.

Jensen EJ, Toon OB, Selkirk HB, Spinhirne JD, Schoeberl MR. 1996. On the formation and persistence of subvisible cirrus clouds near the tropical tropopause. *J. Geophys. Res.* **101**: 21361–21375.

Jiang JH, Livesey NJ, Su H, Neary L, McConnell JC, Richards NA. 2007. Connecting surface emissions, convective uplifting, and long-range transport of carbon monoxide in the upper-troposphere: new observations from the Aura Microwave Limb Sounder. *Geophys. Res. Lett.* **34**: L18812, DOI: 10.1029/2007GL030638.

Jiang JH, Su H, Pawson S, Liu HC, Read W, Waters JW, Santee M, Wu DL, Schwartz M, Livesey N, Lambert A, Fuller R, Lee JN. 2010. Five-year (2004–2009) observations of upper tropospheric water vapor and cloud ice from MLS and comparisons with GEOS-5 analyses. *J. Geophys. Res.* **115**: D15103, DOI: 10.1029/2009JD013256.

Jiang JH, Su H, Zhai C, Perun VS, Del Genio A, Nazarenko LS, Donner LJ, Horowitz L, Seman C, Cole J, Gettelman A, Ringer M, Rotstayn L, Jeffrey S, Wu T, Brient F, Dufresne J-L, Kawai H, Koshiro T, Watanabe M, LÉcuyer TS, Volodin EM, Iversen T, Drange H, Mesquita MS, Read WG, Waters JW, Tian B, Teixeira J, Stephens GL. 2012. Evaluation of cloud and water vapor simulations in CMIP5 Climate Models using NASA A-Train satellite observations. *J. Geophys. Res.* **117**: D1410, DOI: 10.1029/2011JD017237.

Kent GS, Williams ER, Wang PH, McCormick MP, Skeens KM. 1995. Surface temperature related variations in tropical cirrus cloud as measured by SAGE II. *J. Clim.* **8**: 2577–2594.

Kug J-S, Kang I-S. 2006. Interactive feedback between ENSO and the Indian Ocean. *J. Clim.* **19**: 1784–1801.

Kug JS, Sooraj KP, Jin F-F, Luo J-J, Kwon M. 2009. Impact of Indian Ocean dipole on high-frequency atmospheric variability over the Indian Ocean. *Atmos. Res.* **94**(2009): 134–139, DOI: 10.1016/j.atmosres.2008.10.022.

Lee M-A, Yeah C-D, Cheng C-H, Chan J-W, Lee K-T. 2003. Empirical orthogonal function analysis of AVHRR sea surface temperature patterns in Taiwan strait. *J. Mar. Sci. Technol.* **11**(1): 1–7.

Li T, Wang B, Chang CP, Zhang Y. 2003. A theory for the Indian Ocean Dipole–zonal mode. *J. Atmos. Sci.* **60**: 2119–2135.

Lindzen RS. 1990. Some coolness concerning global warming. *Bull. Am. Meteorol. Soc.* **71**: 288–299.

Liou KN. 1986. Influence of cirrus clouds on weather and climate processes: a global perspective. *Mon. Weather Rev.* **114**: 1167–1199.

Liu C, Zipser E, Garrett T, Jiang J, Su H. 2007. How do the water vapor and carbon monoxide "tape recorder" start near the tropical tropopause? *Geophys. Res. Lett.* **34**: L09804, DOI: 10.1029/2006GL029234.

Livesey NJ, Read WG, Lambert A, Cofield RE, Cuddy DT, Froidevaux L, Fuller RA, Jarnot RF, Jiang JH, Jiang YB, Knosp BW, Kovalenko LJ, Pickett HM, Pumphrey HC, Santee ML, Schwartz MJ, Stek PC, Wagner PA, Waters JW, Wu DL. 2007. EOS MLS Version 2.2 and 2.3 Level 2 data quality and description document. JPL Technical Report, D-33509. Jet Propulsion Laboratory: California, CA.

Luo ZJ, Kley D, Johnson RH, Liu GY, Nawrath S, Smit HGJ. 2012. Influence of Sea Surface Temperature on Humidity and Temperature in the Outflow of Tropical Deep Convection. *J. Climate* **25**: 1340–1348.

Massie S, Lowe P, Tie X, Hervig M, Thomas G, Russell J III. 2000. Effect of the 1997 El Nino on the distribution of upper tropospheric cirrus. *J. Geophys. Res.* **105**(D18): 22725–22741.

Masumoto Y, Meyers G. 1998. Forced Rossby waves in the southern tropical Indian Ocean. *J. Geophys. Res.* **103**: 27589–27602.

Meyers G, McIntosh P, Pigot L, Pook M. 2007. The years of El Niño, La Niña, and interactions with the tropical Indian Ocean. *J. Clim.* **20**: 2872–2880.

Perigaud C, Delecluse P. 1993. Interannual sea level variations in the tropical Indian Ocean from Geosat and shallow water simulations. *J. Phys. Oceanogr.* **23**: 1916–1934.

Saji NH, Yamagata T. 2003. Interference of teleconnection patterns generated from the tropical Indian and Pacific Oceans. *Clim. Res.* **25**: 151–169.

Saji NH, Goswami BN, Vinayachandran PN, Yamagata T. 1999. A dipole mode in the tropical Indian Ocean. *Nature* **401**(6751): 360–363.

Schwartz MJ, Lambert A, Manney GL, Read WG, Livesey NJ, Froidevaux L, Ao CO, Bernath PF, Boone CD, Cofield RE, Daffer WH, Drouin BJ, Fetzer EJ, Fuller RA, Jarnot RF, Jiang JH, Jiang YB, Knosp BW, Kruger K, Li J-LF, Mlynczak MG, Pawson S, Russell JM, Santee ML, Snyder WV, Stek PC, Thurstans RP, Tompkins AM, Wagner PA, Walker KA, Waters JW, Wu DL. 2008.

Validation of the Aura Microwave Limb Sounder temperature and geopotential height measurements. *J. Geophys. Res.* **113**: D15S11, DOI: 10.1029/2007JD008783.

Soden BJ, Fu R. 1995. A satellite analysis of deep convection, upper-tropospheric humidity, and the greenhouse effect. *J. Clim.* **8**: 2333–2351.

Stephens GL. 2005. Cloud feedbacks in the climate system: a critical review. *J. Clim.* **18**: 237–273.

Su H, Neelin JD, Chou C. 2001. Tropical teleconnection and local response to SST anomalies during the 1997–1998 El Nino. *J. Geophys. Res.* **106**: 20 025–20 043.

Su H, Read WG, Jiang JH, Waters JW, Wu DL, Fetzer EJ. 2006. Enhanced positive water vapor feedback associated with tropical deep convection: new evidence from Aura MLS. *Geophys. Res. Lett.* **33**: L05709, DOI: 10.1029/2005GL025505.

Su H, Jiang JH, Gu Y, David Neelin J, Kahn BH, Feldman D, Yung YL, Waters JW, Livesey NJ, Santee ML, Read WG. 2008. Variations of tropical upper tropospheric clouds with sea surface temperature and implications for radiative effects. *J. Geophys. Res.* **113**: D10211, DOI: 10.1029/2007JD009624.

Su H, Jiang JH, Stephens GL, Vane DG, Livesey NJ. 2009. Radiative effects of upper tropospheric clouds observed by Aura MLS and CloudSat. *Geophys. Res. Lett.* **36**: L09815, DOI: 10.1029/2009GL037173.

Su H, Jiang JH, Zhai C, Perun VS, Shen JT, Genio AD, Nazarenko LS, Donner LJ, Horowitz L, Seman C, Morcrette C, Petch J, Ringer M, Cole J, Mesquita M, Iversen T, Kristjansson JE, Gettelman A, Rotstayn L, Jeffrey S, Dufresne JL, Watanabe M, Kawai H, Koshiro T, Wu T, Volodin EM, L'Ecuyer T, Teixeira J, Stephens GL. 2013. Diagnosis of regime-dependent cloud simulation errors in CMIP5 models using A-train satellite observations. *J. Geophys. Res.* **118**(7): 2762–2780, DOI: 10.1029/2012JD018575.

Sun D-Z, Lindzen RS. 1993. Distribution of tropical tropospheric water vapor. *J. Atmos. Sci.* **50**: 1643–1660.

Vinayachandran PN, Kurian J, Neema CP. 2007. Indian Ocean response to anomalous conditions during 2006. *Geophys. Res. Lett.* **34**, DOI: 10.1029/2007/GL030194.

Vinayachandran PN, Saji NH, Yamagata T. 1999. Response of the Equatorial Indian Ocean to an unusual wind event during 1994. *Geophys. Res. Lett.* **26**: 1613–1616.

Wang P-H, Minnis P, McCormick MP, Kent GS, Skeens KM. 1996. A 6-year climatology of cloud occurrence frequency from Stratospheric Aerosol and Gas Experiment II observations (1985–1990). *J. Geophys. Res.* **10I**: 29 407–29429.

Webster PJ, Moore AM, Loschnigg JP, Leben RR. 1999. Coupled ocean–atmosphere dynamics in the Indian Ocean during 1997–98. *Nature* **401**(6751): 356–360.

Wu DL, Jiang JH, Read WG, Austin RT, Davis CP, Lambert A, Stephens GL, Vane DG, Waters JW. 2008. Validation of the Aura MLS cloud ice water content measurements. *J. Geophys. Res.* **113**: D15S10, DOI: 10.1029/2007JD008931.

Zhong A, Hendon HH, Alves O. 2005. Indian Ocean variability and its association with ENSO in a global coupled model. *J. Clim.* **18**: 3634–3649.

